Langmuir

Article

pubs.acs.org/Langmuir

Robust Measurement of Membrane Bending Moduli Using Light Sheet Fluorescence Imaging of Vesicle Fluctuations

Andrew F. Loftus,[†] Sigrid Noreng,[‡] Vivian L. Hsieh,[†] and Raghuveer Parthasarathy*[,‡,§]

[†]Department of Chemistry, [‡]Department of Physics, and [§]Materials Science Institute, The University of Oregon, Eugene, Oregon 97403, United States

Supporting Information

ABSTRACT: The mechanical rigidity of lipid membranes is a key determinant of the energetics of cellular membrane deformation. Measurements of membrane bending moduli remain rare, however, and show a large variance, a situation that can be addressed by the development of improved techniques and by comparisons between disparate techniques applied to the same systems. We introduce here the use of selective plane illumination microscopy (SPIM, also known as light sheet fluorescence microscopy) to image thermal fluctuations of giant vesicles. The optical sectioning of SPIM enables high-speed fluorescence imaging of freely suspended vesicles and quantification of edge localization precision, yielding robust fluctuation spectra and rigidity estimates. For both lipid-only membranes and membranes bound by the intracellular trafficking protein Sar1p, which lowers membrane rigidity in a concentration-dependent manner, we show that the resulting bending modulus values are in close agreement with those derived from an independent assay based on membrane tether pulling. We also show that the fluctuation spectra of vesicles bound by the mammalian Sar1A protein, which stiffens membranes at high concentrations, are not well fit by a model of homogeneous quasi-spherical vesicles, suggesting that SPIM-based analysis can offer insights into spatially inhomogeneous properties induced by protein assemblies.

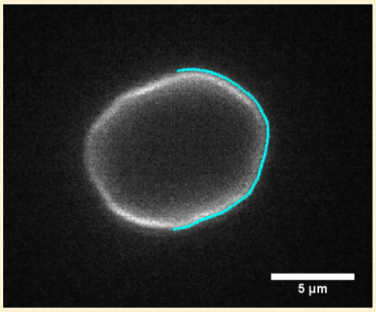

INTRODUCTION

Manipulation of membrane shape is integral to cellular processes as diverse as filipodial extension, mitosis, and intracellular cargo trafficking. In these and other contexts, protein complexes bend membranes into highly curved shapes, the energetics of which are governed in large part by the rigidity, or bending modulus (κ), of the membrane.[1−4] Despite their importance, measurements of membrane rigidity are not common, especially for systems that include membrane-associated proteins as well as lipids. We believe this to be due in large part to a lack, compared to other areas of biophysical research, of development and refinement of measurement techniques and to a lack of cross-validation of disparate techniques. To address this, we show that the combination of light sheet fluorescence microscopy and vesicle fluctuation analysis enables robust measurements of the bending modulus of lipid and protein membranes and that these measurements are in close agreement with values from tether-pulling assays.

Techniques for measuring membrane rigidity generally fall into two categories: (1) tether pulling methods and (2) methods based on shape deformations of giant unilamellar vesicles (GUVs). In the first case, a tubule of membrane is pulled from the bulk by application of a local force, using e.g. a magnetically or optically trapped microparticle or a micropipet.[5] By measuring the tether-associated force and geometry, one can determine the rigidity and tension of the system.[6−8] While insightful and relatively easy to analyze, tether-pulling experiments are low-throughput, requiring significant time to obtain statistically meaningful data.

Experiments involving vesicle deformations usually make use of imaging thermally driven membrane fluctuations.[9−13] The analysis of thermal fluctuation spectra to obtain rigidity and tension is described in refs 14 and 15; more recently, Méléard et al. have extended this approach to incorporate the statistical distribution of mode amplitudes, which significantly improves the robustness of the analysis.[16] Several factors complicate fluctuation-based assays, however. Studies to date have considered giant unilamellar vesicles (GUVs) settled at the bottom of a chamber in order to be close to an imaging objective lens, leading to gravitational shape distortions that complicate the application of quasi-spherical analysis models.[10,13] High-speed imaging of the vesicle membrane is generally provided by phase-contrast microscopy,[13,14,16] making quantitative estimation of the edge localization precision difficult. Moreover, the use of wide-field microscopy techniques limits the ability to visualize membrane-bound proteins, as typical binding affinities are such that discrimination of membrane-bound proteins from unbound background is challenging.

Vesicle-based experiments using electric-field-induced deformations[17,18] involve fitting the change in surface area versus the stress caused by the field to a model of tension-induced

Received: May 31, 2013
Published: November 1, 2013

   dx.doi.org/10.1021/la403837d | *Langmuir* 2013, 29, 14588−14594

suppression of fluctuations. Analysis of these deformations is subject to several assumptions about the form of the electric field, chamber geometry, and vesicle location.[17]

For all of these reasons, values in the literature of the bending modulus of even simple single-component lipid membranes show a large spread. For 1-palmitoyl-2-oleoyl-*sn*-glycero-3-phosphocholine (POPC), for example, discussed below, reported κ values range from 2.5×10^{-20} J[18] to 15.8×10^{-20} J.[10] Moreover, to the best of our knowledge, there are no comparisons of tether-based and vesicle-deformation-based measurements of the same membrane system, either with or without proteins, leaving unanswered the key question of whether the high degree of variation noted above stems from differences in sample preparation or from systematic differences inherent in the various methods.

We aim, therefore, to demonstrate and validate an improved method for measurements of membrane rigidity: the use of selective plane illumination microscopy (SPIM) for vesicle fluctuation imaging. In SPIM, also known as light sheet fluorescence microscopy, a laser is formed into a thin sheet that excites fluorophores in one plane of the sample, the emission from which is imaged onto a camera using a perpendicular objective lens (Figure 1).[19−21] In many recent studies, the fast

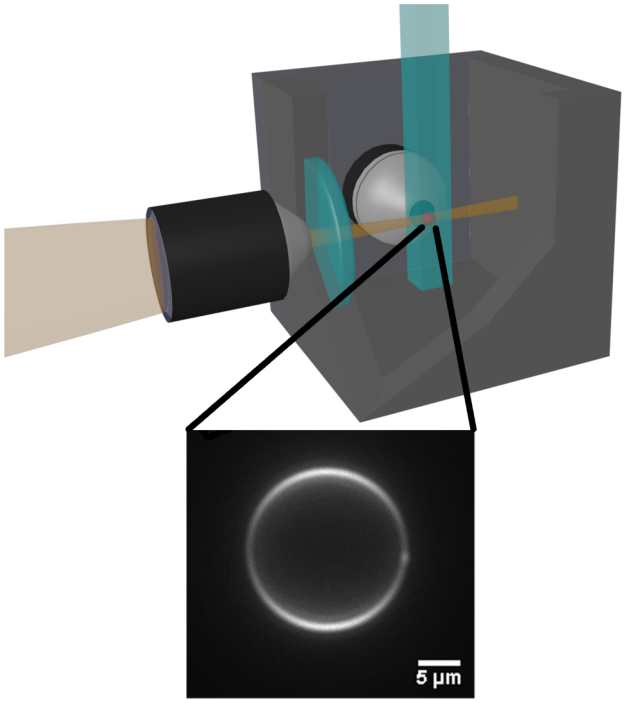

Figure 1. Schematic application of SPIM to image GUVs. A thin sheet of excitation light coincident with the focal plane of an imaging objective allows high-speed optical sectioning of a suspension of lipid vesicles. Inset: image of a POPC vesicle with 2 mol % Texas Red DHPE fluorescent lipids.

three-dimensional imaging and inherent low photon flux that SPIM makes possible have been applied to investigations of animal and plant development.[19,22,23] SPIM has not, however, been previously applied to *in vitro* membrane systems. We realized that SPIM's attributes for multicellular imaging are also ideal for visualizing vesicle fluctuations: Its optical sectioning enables high-speed imaging of the equatorial plane of GUVs, its use of fluorescence provides ring-like images of the vesicle edge (Figure 1B) whose localization precision can be assessed with simple models, and its applicability to thick samples allows the imaging of freely suspended GUVs far from a chamber wall.

We show that SPIM imaging of GUV membrane fluctuations provides data that are well-fit by models of vesicle fluctuation spectra.[16] We measure values for the bending modulus of POPC membranes and membranes bound by various concentrations of the yeast intracellular trafficking protein Sar1p, shown previously to lower membrane rigidity.[24] For each of these systems, SPIM-imaged fluctuation-derived values are in close agreement with values from tether pulling assays (within at most 20%). We also show that the human Sar1A protein, shown previously to increase membrane rigidity and self-associate,[25] gives fluctuation spectra that are not well-fit by a model of homogeneous vesicles.

EXPERIMENTAL METHODS

Lipid Composition. Two lipid membrane mixtures were composed for GUV fluctuation studies: (1) 98 mol % POPC and 2 mol % Texas Red DHPE (1,2-dihexadecanoyl-*sn*-glycero-3-phosphoethanolamine). (2) The "major mix" composition of refs 24 and 26 that mimics the composition of the endoplasmic reticulum membrane, modified to include fluorescent probes and biotinylated lipids, for experiments involving Sar1: 50.5 mol % DOPC (1,2-dioleoyl-*sn*-glycero-3-phosphocholine), 23.0 mol % DOPE (1,2-di(9Z-octadecenoyl)-*sn*-glycero-3-phosphoethanolamine), 11.0 mol % PI (L-α-phosphatidylinositol, from Soy), 8.0 mol % DOPS (1,2-diacyl-*sn*-glycero-3-phosphoserine), 5.0 mol % DOPA (1,2-di(9Z-octadecenoyl)-*sn*-glycero-3-phosphate), 2 mol % Texas Red DHPE, and 0.5 mol % biotinyl-cap-PE (1,2-dihexadecanoyl- *sn*-glycero-3-phosphoethanolamine-*N*-(cap biotinyl)). All lipids were purchased from Avanti Polar Lipids with the exception of Texas Red DHPE, which was purchased from Life Technologies.

Protein Purification and Nucleotide Binding. Sar1 was expressed and purified using protocols similar to those in Barlowe et al.[27] Protein expression was performed with a PTY40 expression vector consisting of a pGEX-2T backbone (GE Healthcare) with inserted GST-Sar1 strain RSB245410 (Sar1p) or RSB3771 (Sar1A) (Schekman Group, UC Berkeley) in BL21 bacterial expression cells. Sar1 was then incubated with a nonhydrolyzable GTP analogue (GMP-PNP (Sigma) or BODIPY-FL GTP-γ-S, thioester (Life Technologies)) prior to the experiment performed as well as EDTA as described previously.[24,25]

Tether Pulling Assays. Tether pulling using an optical trap was performed as previously described in ref 24. Briefly, depositing 5 μL of a 1 mg/mL solution of lipids dissolved in choloroform onto a chambered glass coverslip created multilayered stacks of membrane. The solvent was then dried under vacuum for 5 min, and afterward the lipids were hydrated with 0.2 M HKM buffer (20 mM Hepes-KOH, 160 mM potassium acetate, 1 mM $MgCl_2$, pH 6.8). Sar1p and 100 μM of GMPPNP (Sigma-Aldrich) and 4 mM EDTA were added to the chamber containing the membrane and buffer. After incubating for 5 min, 4.8 μm streptavidin-coated silica microspheres (Bangs Laboratories) were added to the solution. Microspheres were trapped with a home-built optical trap utilizing a 671 nm diode laser set to ≈100 mW of output power. Tethers were pulled from the multilayers by pulling microspheres using the optical trap. The emission from fluorescent lipid probes was imaged using an ORCA-ER CCD camera (Hamamatsu). The fluorescence intensity of the tethers was measured to verify that they consisted of single bilayers, as described in ref 24. Microspheres were imaged with bright field microscopy using a pco.1200 camera (Cooke Corp.) at 100 frames/s. Particle position was tracked with home-built MATLAB programming as previously described.[24,25,28]

Calculation of Bending Rigidity from Membrane Tethers. The retraction of pulled membrane tethers allows determination of the membrane rigidity. As described in refs 24 and 25, the bending rigidity in the absence of spontaneous curvature (κ_0) was calculated from the tether retraction force (f) and tether radius (R_t) using

dx.doi.org/10.1021/la403837d | *Langmuir* 2013, 29, 14588−14594

$$\kappa_0 = \frac{fR_t}{2\pi} \quad (1)$$

The force of the tether is calculated by the relation $f = bv$, where b is the drag coefficient of the system and v is the velocity of the microsphere. The drag coefficient is independently determined for each tether from velocity fluctuations as described generally in Sainis et al.[29] The tether radii were determined from fluorescence images, using Texas Red DHPE fluorescent probes.[24,25]

Vesicle Electroformation. GUVs were created by electroformation as described by Herold et al.[30] Briefly, lipids were deposited on air annealed indium−tin oxide (ITO) glass slides, R_s = 15−25 Ω (Delta Technologies), and dried under vacuum for 10 min. A chamber was assembled from two ITO-glass slides separated by a 1.5 mm gasket of silicon rubber and sealed with binding clips. The electroformation chamber was then gently filled with 0.1 M sucrose solution. After this a sinusoidal ac electric field of 1.2 V_{rms} at 10 Hz was applied to the chamber for 2 h. The GUV suspension was gently pulled out of the chamber with a syringe.

Selective Plane Illumination Microscopy. GUV suspension (10 μL), with or without protein, was placed in a square micro fluorometer cell (Starna Cells) containing 200 μL of 0.25 M sucrose solution. Selective plane illumination microscopy of vesicles was performed using a home-built setup similar to that of ref 19 and described in detail in ref 23. Key components are listed in the Supporting Information (Table S1). Briefly, excitation light for the Texas Red fluorophore labeling lipids was provided by a 594 nm diode laser with a power of 50 mW (Lasermate). The light is passed through an acousto-optic tunable filter and is then incident to a rapidly scanning (2 kHz) galvanometer mirror. A telecentric scan lens transforms the angular scan into a translating scan that passes through a tube lens and objective lens, producing a thin sheet of light in the sample holder. The beam thickness was measured to be 3.0 μm over a lateral extent of ≈100 μm. Images were captured through a 40× 1.0 NA Plan-apo objective lens (Zeiss) perpendicular to the excitation plane and recorded with a 5.5 Mpixel sCMOS camera (pco.edge, Cooke Corp., pixel size 6.5 μm) at an exposure time of 500 μs with a frame rate range of 60−100 frames/s, controlled using home-built software.

The camera exposure time is much smaller than the time scale of the fluctuations of the examined vesicle modes, which are calculated to be over 10 ms up to m = 35 for vesicles of the measured rigidity and radius values,[16] and hence any corrections to the analysis due to finite exposure times will be very small compared to the observed statistical variation between vesicles.

Edge Determination. The location of the vesicle edge was calculated for each two-dimensional image using home-built software written in MATLAB. Starting from a rough, user-input estimation of the center of the vesicle in the initial frame, each image is divided into several (50−300) angular wedges. In each wedge, the vesicle edge is determined by locating the pixels of maximal intensity gradient in the radial direction and then further refined by finding the peak of a local parabolic fit to the intensity gradient.

To determine the precision of this edge determination method, we applied it to simulated images of fluorescent rings with various radii and signal-to-noise ratios (SNRs), mimicking the form of the optically sectioned vesicle images. The difference between the true and estimated edge locations at SNR values corresponding to the experimental SNR gives a measure of the experimental localization precision. The simulated images were created in a similar manner to images of rings described in ref 28; in brief, a high-resolution image of a thin annulus was convolved with the imaging point-spread function, pixelated, and subjected to Poisson-distributed noise. For simulated ring images, we used the theoretical point spread function for the imaging wavelength and numerical aperture, which has a width of 250 nm. We also experimentally measured the PSF by imaging fluorescent beads immobilized in agar gel. Fitting the intensity profiles of beads to a 2D Gaussian yielded PSF widths within 10% of the theoretical value.

The standard deviation of the calculated radial positions of the simulated vesicle edges, which would be zero for perfect edge detection, provides a measure of the image analysis precision. The SNR of experimental images was estimated as the ratio of the peak intensity at the vesicle edge to the standard deviation of the background intensity, and the precision of the edge determination was assessed as the precision of the localization of the simulated images at that SNR.

Calculation of Bending Rigidity from Vesicle Fluctuations. The vesicle edge $\rho(\varphi,t)$, where ρ and φ are the radial and angular coordinates, respectively, from an image obtained at time t is determined as described above. These edge profiles are analyzed to reveal the underlying membrane rigidity and tension using the procedure described in refs 14 and 16. In brief, the angular autocorrelation function

$$\xi(\gamma, t) = \frac{1}{2\pi R^2}\int_{\varphi=0}^{2\pi}[\rho(\varphi+\gamma, t) - \rho(t)][\rho(\varphi + t) - \rho(t)]\,d\varphi \quad (2)$$

where $\rho(t)$ is the mean of ρ, is cosine decomposed

$$\xi(\gamma, t) = \sum_{0<m}^{n_{max}} \chi_m(t)\cos(m\gamma) \quad (3)$$

to give the mode amplitudes χ_m. As described in ref 16, each mode amplitude should follow an exponential (Boltzmann) probability distribution:

$$\Gamma_m(\chi_m) \propto \exp\left[-L_m\frac{\chi_m}{2}\right] \quad (4)$$

where $\Gamma_m(\chi_m)$ is the probability of observing χ_m, and the L_m values (denoted R_m in ref 16) are determined from exponential fits to the measured χ_m distribution over the range for which Γ is at least one-tenth of its maximal value (Figure 2B), to exclude rare outliers.[16]

The L_m values are then fit via least-squares minimization to the expected theoretical form for the mode dependence of quasi-spherical

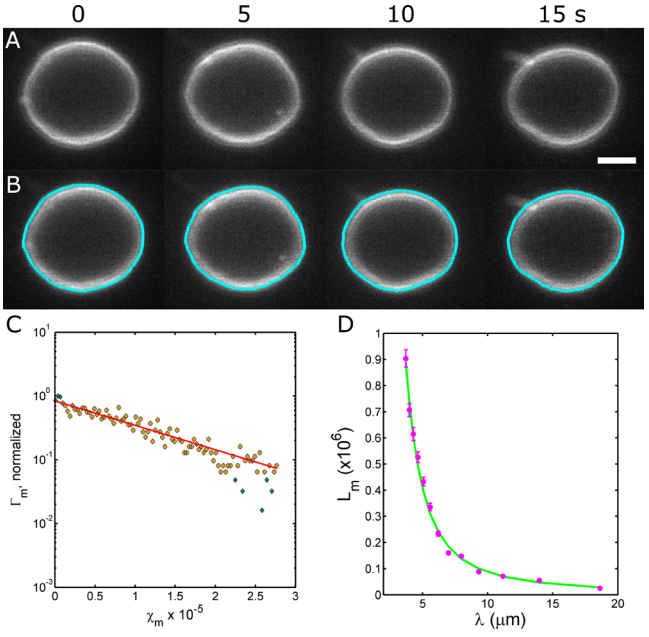

Figure 2. Fluctuation analysis. (A) A series of fluorescence images (Texas Red DHPE) of a lipid vesicle incubated with 3.7 μM Sar1p, with (B) superimposed edges determined from radial gradient maxima. (C) Histogram of autocorrelation amplitudes χ_m for mode m = 4 (λ = 14.0 μm) from 2000 images. The solid line is an exponential fit to the points shown in orange; the uncertainty in the fitted slope is 4%. (D) L_m values (circles) as a function of mode wavelength ($\lambda = 2\pi R/m$) and the best-fit theoretical curve (blue line), which gives a bending modulus $\kappa = (3.1 \pm 0.5) \times 10^{-20}$ J and tension $\sigma = 3.0 \times 10^{-8}$ N/m for this vesicle.

dx.doi.org/10.1021/la403837d | Langmuir 2013, 29, 14588−14594

vesicle fluctuations, for which the rigidity and tension are the two unknown parameters:

$$L_m(\kappa/k_bT, \bar{\sigma}) = \frac{\kappa}{k_bT}\frac{1}{\sum_{n\geq m}^{n_{max}}[Q_n^m(0)]^2/\lambda_n(\bar{\sigma})} \quad (5)$$

where κ is the membrane bending modulus, $\bar{\sigma}$ the reduced membrane tension $\bar{\sigma} = \sigma R^2/\kappa$, k_b being the Boltzmann's constant, $\lambda_n(\bar{\sigma}) = (n + 2)(n - 1)[\bar{\sigma} + n(n + 1)]$, and Q_n^m is given by

$$Q_n^m(\cos\theta) = (-1)^m\sqrt{\frac{2n+1}{4\pi}\frac{(n-m)!}{(n+m)!}}P_n^m(\cos\theta) \quad (6)$$

where $P_n^m(\cos\theta)$ is the associated Legendre function. For individual vesicles, the fit uncertainty for the rigidity is on average 25% of the measured value, ranging from 10 to 55%.

The stated rigidity values are the sample means across distinct vesicles, with the uncertainty given as the standard error of the mean.

Precision of Bending Rigidity Determination. To determine the impact of edge localization precision described above on the determination of κ, we numerically propagated the position uncertainty through the functions that relate position to κ (eqs 2−6). We performed multiple tests in which we replaced the edge positions of vesicles with a random number drawn from a Gaussian distribution centered on the measured position and with a width equal to the localization precision at experimental SNR and then analyzed contour profiles and fluctuation spectra to determine the resulting values of κ. The standard deviation of the resulting κ values provides a measure of the uncertainty due to localization precision.

RESULTS

SPIM imaging of homogeneous giant unilamellar vesicles shows fluctuations whose spectra are well-fit by theoretical models. Figure 2A shows a series of images from one vesicle, together with the image-derived edge positions (Figure 2B, bottom). As expected, the probability distribution of the mode amplitudes $\Gamma_m(\chi_m)$ is exponential (eq 4), yielding a logarithmic slope L_m that decays with mode wavelength $\lambda_m = 2\pi R/m$, where R is the vesicle radius (Figure 2C). The form of $L_m(\lambda_m)$ is well fit by the theoretical expectation for thermal fluctuations of homogeneous quasi-spherical vesicles,[16] illustrated for one vesicle in Figure 2D. Notably, the statistical approach to fluctuation amplitudes introduced in ref 16 (see Experimental Methods) is robust even in the presence of minor imperfections in vesicle morphology, as can be seen in Figure 2. (Less imperfect vesicles were also routinely examined, as represented in Figure S1.)

SPIM-based fluctuation analysis of lipid-only vesicles composed of 98% POPC (see Experimental Methods) yields spectra that are well fit by expected theoretical forms (e.g., Figure S2), yielding an average rigidity value over $N = 32$ vesicles of $\kappa = (12.1 \pm 1.9) \times 10^{-20}$ J. Moreover, we are able to measure bilayer rigidity using a completely independent technique, the pulling of membrane tethers from lipid multilayers.[6−8,24,31] A brief summary of the method of tether pulling using optically trapped microspheres, and the associated analysis, is given in the Experimental Methods section. These measurements of POPC lipids yield a value of $\kappa = (10.6 \pm 1.7) \times 10^{-20}$ J. Notably, the two techniques give similar values, within their uncertainties of each other. We find that the average vesicle tension is 1.45×10^{-7} N/m with a standard deviation of 3.30×10^{-7} N/m, in the range generally observed for electroformed vesicles.[13]

As detailed in the Experimental Methods, fluorescence imaging of vesicle edges allows quantification of the precision of radial position determination via examination of simulated vesicle images. The experimental signal-to-noise ratios for the vesicle edges are in the range 5−20; regions of brighter and dimmer intensity are due to the geometry-dependent angle between the excitation dipole of the Texas Red fluorophore, which orients in the plane of the lipid bilayer,[32] and the linearly polarized excitation laser light. These SNRs give an average precision of ≈10 nm. As described in the Experimental Methods, this results in a localization-based uncertainty in κ of $\approx 0.1 \times 10^{-20}$ J, which is small compared to the statistical variation in rigidity between vesicles (Figure 3).

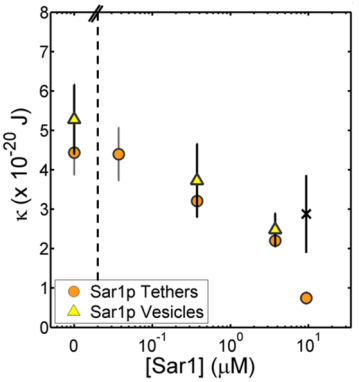

Figure 3. Membrane rigidity determined from tether-pulling studies (orange circles, reported previously in Settles et al.[24]), and vesicle fluctuations (yellow triangles), as a function of Sar1p concentration. The two independent techniques give similar rigidity values. At high protein concentration (≈10 μM), spontaneous tubulation and budding of the majority of vesicles prevents fluctuation analysis; the plotted rigidity (black ×) is derived from the minority of nontubulating vesicles and so is likely an upper bound on rigidity.

We next present rigidity measurements based on light sheet fluctuation imaging of a system for which earlier tether-based measurements demonstrated protein-induced modulation of membrane rigidity, namely the intracellular trafficking protein Sar1p binding to "major mix" lipids that mimic the composition of the endoplasmic reticulum.[24] As shown in Figure 2, GUVs incubated with Sar1p show fluctuation behavior that is well fit by conventional theory. In Figure 3 we plot the previously obtained tether-derived measurements together with new vesicle-based values. We provide movies of representative vesicles incubated with 0 and 3.7 μM Sar1p as Supporting Information Videos 1 and 2, respectively. From 0 to 4 μM Sar1p, rigidity values from the two techniques are very similar. At 9 μM Sar1p (black ×, Figure 3), many vesicles had disintegrated, forming multiple tubules or budding daughter vesicles, and so could not be analyzed in the framework of quasi-spherical vesicle fluctuations.[16] The data point shown at 9 μM Sar1p is from a small number ($N = 6$) of intact vesicles, which were a minority of those found in solution, and so should be considered an upper bound for the rigidity.

In our previous work we showed that the mammalian paralogs of Sar1, Sar1A and Sar1B, lower membrane rigidity at low concentrations but raise it at concentrations above ≈10 μM.[25] However, tether-based rigidity measurements were difficult at higher concentrations because tethers were often impossible to pull, presumably because the force required exceeded the available optical trapping strength. Imaging vesicle fluctuations allowed estimation of membrane rigidity in the presence of high concentrations of the mammalian Sar1 proteins. For example, rigidity at 36 μM Sar1A was on average $\approx 30 \times 10^{-20}$ J, over 6 times that of the lipid bilayer in the

dx.doi.org/10.1021/la403837d | Langmuir 2013, 29, 14588−14594

absence of protein and approximately 2 times the maximum value that could be probed by tether-based investigations.

An additional attribute of fluctuation analysis is that the form of the fluctuation spectra provides information about possible scale-dependent vesicle mechanics. For Sar1A, the L_m values are not well fit by the theoretical expression for homogeneous, quasi-spherical vesicles (Figure 4A; compare with Figure 2C for

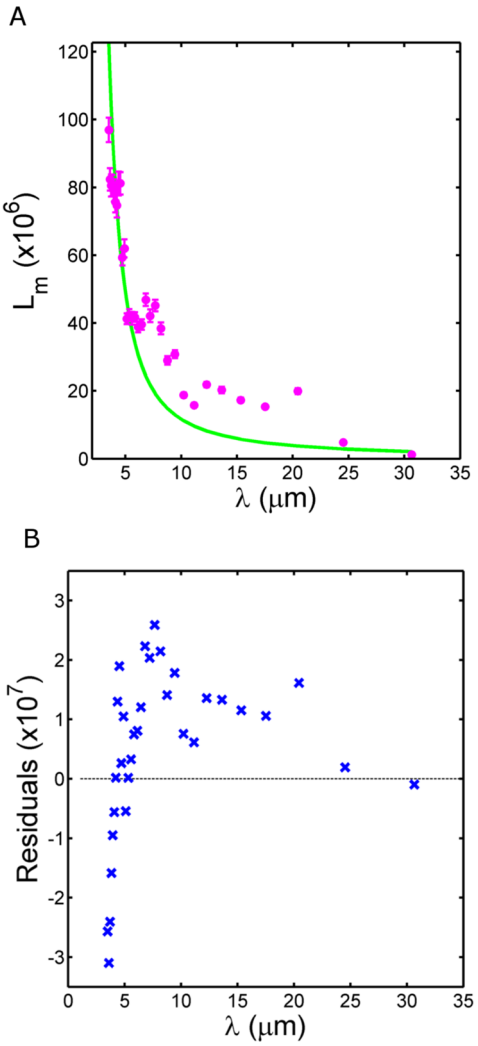

Figure 4. (A) L_m as a function of mode wavelength for a vesicle incubated with 36 μM Sar1A. The data poorly fit the expected form for fluctuations of homogeneous quasi-spherical vesicles (solid curve, rigidity 26×10^{-20} J). (B) Residuals of the fit in (A). The data show a nonrandom form implying a systematic deviation from the expected theory.

Sar1p) and show nonrandom deviation from the expected form (Figure 4B). Notably, the individual χ_m remain exponentially distributed (Figure S3), as would be expected for thermally driven modes.

SUMMARY

We have demonstrated the utility of using light sheet fluorescence microscopy and thermal fluctuation analysis for measuring membrane bending moduli. SPIM provides several advantages over conventional fluctuation imaging due to its use of fluorescent probes, enabling quantifiably precise edge determination, and its applicability to freely suspended vesicles, avoiding gravitational distortions at chamber walls. With this approach, we find a bending modulus for POPC membranes of $\kappa = (12.1 \pm 1.9) \times 10^{-20}$ J, indistinguishable within uncertainty of the value determined by the independent technique of membrane tether pulling. The concordance is especially notable given the large spread of rigidity values for POPC noted in the literature, ranging from 2.5×10^{-20} to 15.8×10^{-20} J (Table 1).

Table 1. Bending Modulus for POPC Membrane Assays in the Literature

reference	bending modulus ($\times 10^{-20}$ J)	method
18	2.47 ± 0.49	vesicle deformation
9	3.96 ± 0.87	fluctuation analysis
9	5.89 ± 1.18	vesicle deformation
33	6.70 ± 2.00	tethers using atomic force microscopy
10	13.00 ± 0.40	fluctuation analysis
11	15.80 ± 0.33	fluctuation analysis
34	3.27 ± 0.19	vesicle deformation
12	9.87 ± 0.30	fluctuation analysis
16	12.9 ± 0.04	fluctuation analysis
this work	12.1 ± 1.9	fluctuation analysis
this work	10.6 ± 1.7	tether pulling

For protein-bound membranes, we similarly find a close agreement between fluctuation-derived and tether-derived bending modulus values (Figure 3). Notably, our results provide the first reported comparisons of rigidity measurements using vesicle-based and non-vesicle-based techniques by the same group applied to the same systems, and the similarity of the outcomes suggests membrane rigidity may be more robustly measurable than the existing literature would imply.

Our vesicle fluctuation imaging also highlights two sorts of systems for which this approach can fail. For high concentrations of the membrane-softening protein Sar1p,[24] disintegration of vesicles leaves only a small and non-representative fraction left for analysis. For high concentrations of the rigidity-enhancing Sar1A,[25] the observed fluctuation spectrum is not well fit by theory (Figure 4A). Given prior observations of low diffusion rates at high concentrations that led to a model of weak interprotein binding by Sar1A,[25] this may suggest a picture of a protein mesh such that below the characteristic mesh size, the effective rigidity is similar to that of the lipid membrane, and above, it takes a larger value characteristic of the protein network. Investigating this model will require not only more experimental work but also a better theoretical understanding of the fluctuation spectra that should arise for inhomogeneous quasi-spherical vesicles. For both simple and complex membrane systems, however, we believe that light-sheet-based fluctuation analysis provides a powerful route to characterizing membrane physical properties.

Still more broadly, we introduce the application of light sheet fluorescence microscopy to studies of membrane biophysics. This imaging technique has attracted a great deal of attention in recent years due to the insights it allows into embryonic development.[19−23] Its utility for nonliving systems has been remarkably unrealized, however, and we look forward to its further applications to dynamic interfaces and soft materials.

dx.doi.org/10.1021/la403837d | Langmuir 2013, 29, 14588−14594

■ ASSOCIATED CONTENT

Supporting Information

Table of selective plane illumination microscopy components (Table S1); supporting captions and figures of fluorescence images of giant vesicles (Figure S1), fluctuation analysis of a representative POPC vesicle (Figure S2), and histograms of autocorrelation amplitudes for a vesicle incubated with 36 μM Sar1A (Figure S3); movies from light sheet fluorescence imaging of a (Video S1) Major Mix vesicle and (Video S2) Major Mix vesicle incubated with 3.7 μM Sar1p. This material is available free of charge via the Internet at http://pubs.acs.org.

■ AUTHOR INFORMATION

Corresponding Author

*E-mail raghu@uoregon.edu; Ph 541-346-2933; Fax 541-346-5861 (R.P.).

Notes

The authors declare no competing financial interest.

■ ACKNOWLEDGMENTS

We thank Karen Kallio and Jim Remington for assistance with protein expression and Bob Lesch and Randy Schekman for providing plasmids for Sar1A. We also thank Mike Taormina and Matthew Jemielita for assistance with SPIM techniques. This work was supported by National Science Foundation Awards 0922951 and 1006171.

■ REFERENCES

(1) Parthasarathy, R.; Groves, J. T. Curvature and spatial organization in biological membranes. *Soft Matter* **2007**, *3*, 24−33.

(2) McMahon, H. T.; Gallop, J. L. Membrane curvature and mechanisms of dynamic cell membrane remodeling. *Nature* **2005**, *438*, 590−596.

(3) Tanaka-Takiguchi, Y.; Itoh, T.; Tsujita, K.; Yamada, S.; Yanagisawa, M.; Fujiwara, K.; Yamamoto, A.; Ichikawa, M.; Takiguchi, K. Endocytosis-like uptake of surface-modified drug nanocarriers into giant unilamellar vesicles. *Langmuir* **2012**, *29*, 328−336.

(4) Baumgart, T.; Capraro, B. R.; Zhu, C.; Das, S. L. Thermodynamics and mechanics of membrane curvature generation and sensing by protein and lipids. *Annu. Rev. Phys. Chem.* **2011**, *62*, 483−506.

(5) Rossier, O.; Cuvelier, D.; Borghi, N.; Puech, P. H.; Derényi, I.; Buguin, A.; Nassoy, P.; Brochard-Wyart, F. Giant vesicles under flows: Extrusion and retraction of tubes. *Langmuir* **2003**, *19*, 575−584.

(6) Waugh, R. E.; Hochmuth, R. M. Mechanical equilibrium of thick, hollow, liquid membrane cylinders. *Biophys. J.* **1987**, *52*, 391−400.

(7) Dai, J.; Sheetz, M. P. Mechanical properties of neuronal growth cone membranes studied by tether formation with laser optical tweezers. *Biophys. J.* **1995**, *68*, 988−996.

(8) Raucher, D.; Sheetz, M. P. Characteristics of a membrane reservoir buffering membrane tension. *Biophys. J.* **1999**, *77*, 1992−2002.

(9) Niggemann, G.; Kummrow, M.; Helfrich, W. The bending rigidity of phosphatidylcholine bilayers: dependences on experimental method, sample cell sealing and temperature. *J. Phys. II* **1995**, *5*, 413−425.

(10) Henriksen, J.; Rowat, A.; Ipsen, J. Vesicle fluctuation analysis of the effects of sterols on membrane bending rigidity. *Eur. Biophys. J.* **2004**, *33*, 732−741.

(11) Bouvrais, H.; Pott, T.; Bagatolli, L. A.; Ipsen, J. H.; Méléard, P.; Bouvrais, H.; Pott, T.; Bagatolli, L. A.; Ipsen, J. H.; Méléard, P. Impact of membrane-anchored fluorescent probes on the mechanical properties of lipid bilayers. *Microsc. Imaging Membr. Domains* **2010**, *1798*, 1333−1337.

(12) Bouvrais, H.; Méléard, P.; Pott, T.; Jensen, K. J.; Brask, J.; Ipsen, J. H. Softening of POPC membranes by magainin. *Biophys. Chem.* **2008**, *137*, 7−12.

(13) Pécréaux, J.; Döbereiner, H.-G.; Prost, J.; Joanny, J.-F.; Bassereau, P. Refined contour analysis of giant unilamellar vesicles. *Eur. Phys. J. E* **2004**, *13*, 277−290.

(14) Faucon, J. F.; Mitov, M. D.; Méléard, P.; Bivas, I.; Bothorel, P. Bending elasticity and thermal fluctuations of lipid membranes. Theoretical and experimental requirements. *J. Phys. (Paris)* **1989**, *50*, 2389−2414.

(15) Méléard, P.; Gerbeaud, C.; Pott, T.; Fernandez-Puente, L.; Bivas, I.; Mitov, M. D.; Dufourcq, J.; Bothorel, P. Bending elasticities of model membranes: influences of temperature and sterol content. *Biophys. J.* **1997**, *72*, 2616−2629.

(16) Méléard, P.; Pott, T.; Bouvrais, H.; Ipsen, J. H. Advantages of statistical analysis of giant vesicle flickering for bending elasticity measurements. *Eur. Phys. J. E* **2011**, *34*, 1−14.

(17) Gracia, R. S.; Bezlyepkina, N.; Knorr, R. L.; Lipowsky, R.; Dimova, R. Effect of cholesterol on the rigidity of saturated and unsaturated membranes: fluctuations and electrodeformation analysis of giant vesicles. *Soft Matter* **2010**, *6*, 1472−1482.

(18) Kummrow, M.; Helfrich, W. Deformation of giant lipid vesicles by electric fields. *Phys. Rev.* **1991**, *44*, 8356−8360.

(19) Keller, P. J.; Schmidt, A. D.; Wittbrodt, J.; Stelzer, E. H. K. Reconstruction of zebrafish early embryonic development by scanned light sheet microscopy. *Science* **2008**, *322*, 1065−1069.

(20) Huisken, J.; Stainier, D. Y. R. Selective plane illumination microscopy techniques in developmental biology. *Development* **2009**, *136*, 1963−1975.

(21) Ntziachristos, V. Going deeper than microscopy: the optical imaging frontier in biology. *Nat. Methods* **2010**, *7*, 603−614.

(22) Jemielita, M.; Taormina, M. J.; DeLaurier, A.; Kimmel, C. B.; Parthasarathy, R. Comparing phototoxicity during the development of a zebrafish craniofacial bone using confocal and light sheet microscopy techniques. *J. Biophotonics* **2012**, DOI: 10.1002/jbio.201200144.

(23) Taormina, M. J.; Jemielita, M.; Stephens, W. Z.; Burns, A. R.; Troll, J. V.; Parthasarathy, R.; Guillemin, K. Investigating bacterial-animal symbioses with light sheet microscopy. *Biol. Bull.* **2012**, *223*, 7−20.

(24) Settles, E. I.; Loftus, A. F.; McKeown, A. N.; Parthasarathy, R. The vesicle trafficking protein Sar1 lowers lipid membrane rigidity. *Biophys. J.* **2010**, *99*, 1539−1545.

(25) Loftus, A. F.; Hsieh, V. L.; Parthasarathy, R. Modulation of membrane rigidity by the human vesicle trafficking proteins Sar1A and Sar1B. *Biochem. Biophys. Res. Commun.* **2012**, *426*, 585−589.

(26) Matsuoka, K.; Orci, L.; Amherdt, M.; Bednarek, S. Y.; Hamamoto, S.; Schekman, R.; Yeung, T. COPII-coated vesicle formation reconstituted with purified coat proteins and chemically defined liposomes. *Cell* **1998**, *93*, 263−275.

(27) Barlowe, C.; d' Enfert, C.; Schekman, R. Purification and characterization of Sar1p, a small GTP-binding protein required for transport vesicle formation from the endoplasmic reticulum. *J. Biol. Chem.* **1993**, *268*, 873−879.

(28) Parthasarathy, R. Rapid, accurate particle tracking by calculation of radial symmetry centers. *Nat. Methods* **2012**, *9*, 724−726.

(29) Sainis, S. K.; Germain, V.; Dufresne, E. R. Statistics of Particle Trajectories at Short Time-Intervals Reveal fN-Scale Colloidal Forces. *Phys. Rev. Lett.* **2007**, *99*, 018303.

(30) Herold, C.; Chwastek, G.; Schwille, P.; Petrov, E. P. Efficient electroformation of supergiant unilamellar vesicles containing cationic lipids on ITO-coated electrodes. *Langmuir* **2012**, *28*, 5518−5521.

(31) Borghi, N.; Brochard-Wyart, F. Tether extrusion from red blood cells: integral unbinding from cytoskeleton. *Biophys. J.* **2007**, *93*, 1369−1379.

(32) Groves, J. T.; Parthasarathy, R.; Forstner, M. B. Fluorescence imaging of membrane dynamics. *Annu. Rev. Biomed. Eng.* **2008**, *10*, 311−338.

(33) Kocun, M.; Janshoff, A. Pulling tethers from pore-spanning bilayers: Towards simultaneous determination of local bending modulus and lateral tension of membranes. *Small* **2012**, *8*, 847−851.
(34) Solmaz, M. E.; Biswas, R.; Sankhagowit, S.; Thompson, J. R.; Mejia, C. A.; Malmstadt, N.; Povinelli, M. L. Optical stretching of giant unilamellar vesicles with an integrated dual-beam optical trap. *Biomed. Opt. Express* **2012**, *3*, 2419−2427.